Research Article

INTERNATIONAL JOURNAL OF ADVANCED ROBOTIC SYSTEMS

International Journal of Advanced Robotic Systems
May-June 2019: 1–11

DOI: 10.1177/1729881419852813
journals.sagepub.com/home/arx
SAGE

Design of a micro pole-climbing robot

Du Qiaoling[1], Li Yan[2] and Liu Sinan[1]

Abstract

Pole-climbing robots are increasingly needed to carry out high-risk tasks for human beings. A micro pole-climbing robot is designed in this article. A strategy of climbing pole is proposed, which has high precision in each stride. To enable the robot to sample the angle relative to the ground in real time, micro electro mechanical systems (MEMS) three-axis accelerometers are equipped on micro pole-climbing robot. Accelerometer measurements provide an absolute reference for the pitch-and-roll components of the estimated orientation, which are used as feedback input signal of proportional–integral–derivative algorithm. A supporting structure is installed at the joint of each gripper to assist the robot to clamp a pole. The support structure improves the load capacity of the robot. The maximum load of micro pole-climbing robot is 3.5 times its own weight. The climbing pole strategy includes the following sections: a Denavit–Hartenberg model is established and the inverse kinematic solution is analyzed; the flip locomotion is analyzed; and the parameters of K_P, K_I, and K_D in the proportional–integral–derivative control method are obtained according to the Ziegler–Nichols controller. The performance of pole climbing based on micro pole-climbing robot prototype was tested. By using this strategy of climbing pole, the self-continuous climbing with controllable stride is realized, and the angular velocity fluctuation of the five-bar mechanism driven by steering gear is reduced. The average time of a single step is 27 s, the maximum relative error of step distance is 4.6%, and the average relative error is 2.8%. These results confirm that the structure scheme and the strategy of climbing pole are feasible.

Keywords

Five-bar linkage, pole-climbing robot, kinematic model, PID, autonomous climbing

Date received: 31 October 2018; accepted: 30 April 2019

Topic: Climbing and Walking Robots
Topic Editor: Yannick Aoustin
Associate Editor: Cedric Clevy

Introduction

Aerial work to climb poles,[1–5] trees,[6,7] or trusses[8–10] can result in worker injuries[11,12] due to human kinematic and spatial limitations. Pole-climbing robots are therefore increasingly wanted to carry out high-risk tasks for human beings. There are many studies about pole-climbing robots with significant achievements.[1–5,6–10,13–24] Autonomous climbing is a necessity for these robots as the operators may not see the next target to be grasped by the robots all the times.

RoMeLa Robot & Mech Lab designed a serpentine robot called HyDRAS,[1] which comprises a serial chain of actuated universal joints for pole climbing. HyDRAS can wrap its body around the structure in a helical shape and rotates its body along its own central body axis to roll up the structure. Haynes et al. made a type of legged robot—RiSE V3.[2] RiSE V3 is used for dynamical, high-speed

[1] State Key Laboratory on Integrated Optoelectronics, College of Electronic Science and Engineering, Jilin University, Changchun, Jilin, China
[2] College of Mechanical Engineering, Jilin Engineering Normal University, Changchun, Jilin, China

Corresponding author:
Du Qiaoling, State Key Laboratory on Integrated Optoelectronics, College of Electronic Science and Engineering, Jilin University, Changchun, Jilin 130012, China.
Email: duql@jlu.edu.cn

climbing of a uniformly convex cylindrical structure. It weighs 5.4 kg and is 70 cm long plus a 28 cm tail appendage. Faizal et al. developed a tree-climbing robot to carry its weight by using two servo motors.[6] The robot can only climb the trees with a diameter not larger than 10 cm. Another climbing robot designed by the Chinese Academy of Forestry can climb trees of multiple diameters.[7] Taking a modular approach, a biped-climbing robot (Climbot) was constructed.[13] Climbot implements autonomous climbing with three basic gaits suitable for different occasions. A pole-climbing robot for transmission line was also built. It adsorbs and locates by an electromagnet module, so it can only climb on metal surfaces.[3] Zahra et al. made an electrical pole-climbing robot, which has a good spatial member transition ability, but its size is relatively large.[4] A robot prototype was developed to construct overhead distribution lines in Quebec hydropower stations.[5]

The pole-climbing robot Pobot V2 was based on the innovative principle of rolling self-locking[8]; it uses no energy to maintain itself at a given altitude. There are also a few prototype robots for truss climbing.[9,10,14] Shady3D built by MIT[10] can move along a three-dimensional (3-D) truss structure. The stability of gripping truss is solved, but the shape of truss section is required. The feasible single-step collision-free climbing motion of BiPCRs in space truss was proposed.[15] The 3-D Climber climbing robot developed by Tavakoli et al.[17] is suitable for climbing pipelines. It has a strong maneuverability but with a large size and a slow movement. The robot is designed to crawl or descend with three wheels—two free wheels and one driving wheel.[18]

Some robots can do automatic pole climbing. However, there are few discussions on the accuracy of the robot's climbing steps. This article describes a micro pole-climbing robot (MPCRobot) and proposed a strategy of climbing pole. By using this strategy of climbing pole, the self-continuous climbing with controllable stride is realized, and the angular velocity fluctuation of the five-bar mechanism driven by steering gear is reduced.

Pole-climbing robot architecture

The 3-D model of MPCRobot is shown in Figure 1. It consists of five bar linkages of a_0, a_1, a_2, a_3, and a_4; four joints of j_0, j_1, j_2, and j_3; two supports of h_1 and h_2; and two grippers of g_1 and g_2. The functions of j_0 and j_3 are to adjust the angle of the robot fuselage and grasp, and the functions of j_1 and j_2 are to adjust the stride distance. The supporting structures of h_1 and h_2 are formed between the support frame under the gripper and the pole, making MPCRobot stable as a whole.

The coordinated actions of a_1, a_2, and a_3 determine the stride of the robot during the overturning process, and a_0 and a_4 transmit the distance to the two graspers g_1 and g_2 without taking part in the determination of the step size. When a_0 and a_4 rotate to each other parallel, the distance between g_1 and g_2 is exactly equal to the stride determined by a_1, a_2, and a_3 according to the geometric relationship of the parallelogram.

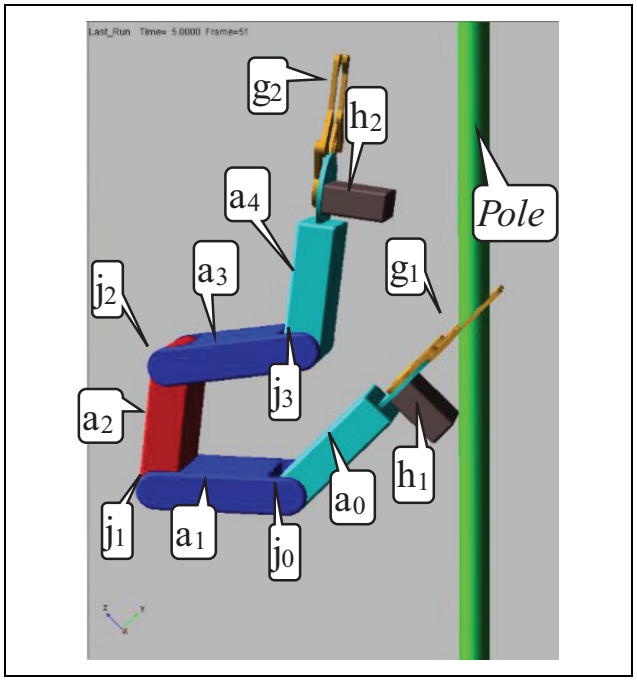

Figure 1. 3-D model of the micro pole-climbing robot. 3-D: three-dimensional.

The advantage of this design is that the structure only needs a_0 and a_4 to keep parallel with each other and does not require g_1 and g_2 to keep strictly perpendicular to the climbing pole, which simplifies the design of the grippers and also reduces the clamping force of the grippers.

Modelling and analysis

In Figure 1, a_0 and g_1 and a_4 and g_2 are fixed connections, which are represented by l_1 and l_2, respectively. The fixed angle γ_1 is formed between l_1 and the pole due to the support h_1. MPCRobot rotates j_0, j_1, and j_2 to make j_3 move to Q in order to realize the stride action according to the preset step size D. Rotation j_3 makes l_2 reach a certain posture, and then γ_2 ($\gamma_2 = \gamma_1$) between l_2 and the pole is formed and then D is parallel to the pole, as shown in Figure 2. In the process, S is regarded as the starting point of the motion as the fixed point, and the control process is to adjust the angle of j_0, j_1, and j_2 to make j_3 reach the target Q.

D-H parameter model

The Denavit–Hartenberg (D-H) coordinate system of MPCRobot is established, as shown in Figure 2. The coordinate system of j_0 is represented by x_0–z_0. The coordinate systems of j_1, j_2, and j_3 are established in turn, such as x_1–z_1, x_2–z_2, and x_3–z_3. The parameters are presented in Table 1.

$\theta_i (i = 1, 2, 3)$ is the angle of linkage, D is the distance between j_0 and j_3, $a_i (i = 1, 2, 3)$ is the length of each common perpendicular line, and ∂ is the angle between the axis of the joint.

Kinematics analysis

The general transformation matrix of the two joint coordinate systems can be described as follows

$$T_{i+1} = \begin{bmatrix} \cos\theta_{i+1} & -\sin\theta_{i+1}\cos\partial_{i+1} & \sin\theta_{i+1}\sin\partial_{i+1} & a_{i+1}\cos\theta_{i+1} \\ \sin\theta_{i+1} & \cos\theta_{i+1}\cos\partial_{i+1} & -\cos\theta_{i+1}\sin\partial_{i+1} & a_{i+1}\sin\theta_{i+1} \\ 0 & \sin\partial_{i+1} & \cos\partial_{i+1} & d_{i+1} \\ 0 & 0 & 0 & 1 \end{bmatrix} \quad (1)$$

Set $S_i = \sin\theta_i$, $C_i = \cos\theta_i$, $C_{123} = \cos(\theta_1 + \theta_2 + \theta_3)$, $S_{123} = \sin(\theta_1 + \theta_2 + \theta_3)$, $i = 1, 2, 3$, then the rotation matrices T_1, T_2, and T_3 can be obtained

$$T_1 = \begin{bmatrix} C_1 & -S_1 & 0 & a_1C_1 \\ S_1 & C_1 & 0 & a_1S_1 \\ 0 & 0 & 1 & 0 \\ 0 & 0 & 0 & 1 \end{bmatrix}$$

$$T_2 = \begin{bmatrix} C_2 & -S_2 & 0 & a_2C_2 \\ S_2 & C_2 & 0 & a_2S_2 \\ 0 & 0 & 1 & 0 \\ 0 & 0 & 0 & 1 \end{bmatrix} \quad (2)$$

$$T_3 = \begin{bmatrix} C_3 & -S_3 & 0 & a_3C_3 \\ S_3 & C_3 & 0 & a_3S_3 \\ 0 & 0 & 1 & 0 \\ 0 & 0 & 0 & 1 \end{bmatrix}$$

Let the D-H coordinate system of the end of a_3 be N. When the stride distance D is perpendicular to the ground, it is obvious that $p_y = p_z = 0$, $p_x = D$. Transformation matrix from end gripper to pedestal can be obtained by equation (3)[23]

$$\begin{aligned} N &= T_1 \times T_2 \times T_3 \\ &= \begin{bmatrix} C_{123} & -S_{123} & 0 & a_1C_1 + a_2C_{12} + a_3C_{123} \\ S_{123} & C_{123} & 0 & a_1S_1 + a_2S_{12} + a_3S_{123} \\ 0 & 0 & 1 & 0 \\ 0 & 0 & 0 & 1 \end{bmatrix} \\ &= \begin{bmatrix} n_x & o_x & a_x & p_x \\ n_y & o_y & a_y & p_y \\ n_z & o_z & a_z & p_z \\ 0 & 0 & 0 & 1 \end{bmatrix} = \begin{bmatrix} n_x & o_x & a_x & d \\ n_y & o_y & a_y & 0 \\ n_z & o_z & a_z & 0 \\ 0 & 0 & 0 & 1 \end{bmatrix} \end{aligned} \quad (3)$$

Inverse kinematics solutions θ_1, θ_2, and θ_3

The inverse kinematics of the end effector is solved by using T_1^{-1} left multiplier equation (3), as shown below[24]

$$\begin{aligned} &T_1^{-1}N = T_1^{-1}T_1T_2T_3 \\ &\begin{bmatrix} C_{23} & -S_{23} & 0 & a_3C_{23} + a_2C_2 \\ S_{23} & C_{23} & 0 & a_3S_{23} + a_2S_2 \\ 0 & 0 & 1 & 0 \\ 0 & 0 & 0 & 1 \end{bmatrix} = \begin{bmatrix} n_xC_1 + n_yS_1 & o_xC_1 + o_yS_1 & a_xC_1 + a_yS_1 & p_xC_1 + p_yS_1 - a_1 \\ n_yC_1 - n_xS_1 & o_yC_1 - o_xS_1 & a_yC_1 - a_xS_1 & p_yC_1 - p_xS_1 \\ n_z & o_z & a_z & p_z \\ 0 & 0 & 0 & 1 \end{bmatrix} \end{aligned} \quad (4)$$

Assuming θ_1 is known and setting $m = p_xC_1 + p_yS_1 - a_1$ and $n = p_yC_1 - p_xS_1$, then equations (5) and (6) can be obtained by equation (4). Equation (7) can be obtained by equations (3) and (4) square sum.

$$m = a_3C_{23} + a_2C_2 \quad (5)$$

$$n = a_3S_{23} + a_2S_2 \quad (6)$$

$$m^2 + n^2 + a_3^2 - 2a_3(mC_{23} + nS_{23}) = a_2^2 \quad (7)$$

Set $k = mC_{23} + nS_{23}$, then

$$k = \frac{m^2 + n^2 + a_3^2 - a_2^2}{2a_3} \quad (8)$$

Equation (9) can be obtained by using the universal formula of trigonometric function. Then θ_{23} can be

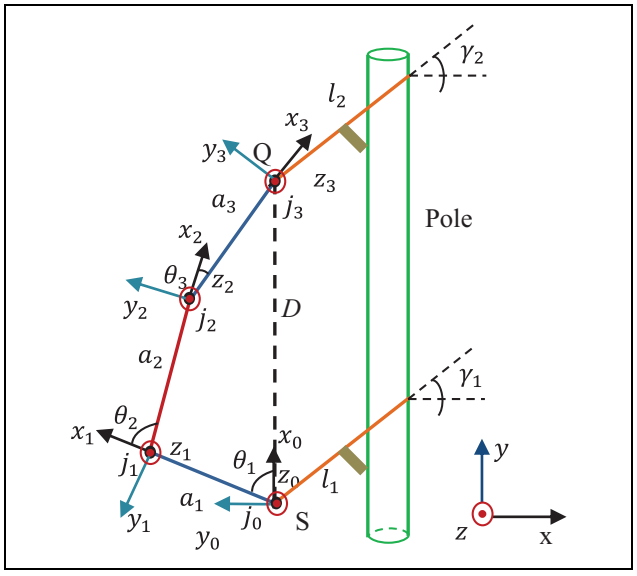

Figure 2. D-H coordinate system of MPCRobot. D-H: Denavit–Hartenberg; MPCRobot: micro pole-climbing robot.

Table 1. Parameters of D-H coordinate system of MPCRobot.

#	θ	d	a	∂
0–1	θ_1	0	a_1	0
1–2	θ_2	0	a_2	0
2–3	θ_3	0	a_3	0

D-H: Denavit–Hartenberg; MPCRobot: micro pole-climbing robot.

obtained as shown in equation (10). θ_2 can be obtained by substituting equation (10) into equation (6) as shown in equation (11). Finally, θ_3 can be obtained by equations (10) and (11)

$$m + k\tan^2\frac{\theta_2+\theta_3}{2} - 2n\tan\frac{\theta_2+\theta_3}{2} + k - m = 0 \quad (9)$$

$$\theta_{23} = \theta_2 + \theta_3 = 2\arctan\frac{n \pm \sqrt{n^2 - k^2 + m^2}}{m+k} \quad (10)$$

$$\theta_2 = \arcsin\frac{n - a_3\sin(\theta_2+\theta_3)}{a_2} \quad (11)$$

$$\theta_3 = 2\arctan\frac{n \pm \sqrt{n^2 - k^2 + m^2}}{m+k} - \theta_2 \quad (12)$$

In addition, the inverse trigonometric function has only one root in the definition domain $\left(-\frac{\pi}{2}, \frac{\pi}{2}\right)$, and there is actually another root in the whole coordinate plane $(-\pi, \pi)$, so another root should be complemented. For the cosine function solution θ, another root $\pi - \theta$ should be complemented. For the arc tangent solution θ, root $\pi + \theta$ should be complemented.

In the inverse kinematic solutions, there are two kinds of solutions which should be abandoned: the wrong mathematical solutions and the infeasible solutions of the system. The wrong mathematical solutions occur because of simultaneous squaring steps on both sides of equation (7). This transformation produces some wrong roots. Such wrong solutions are eliminated by bringing back the original equation. The infeasible solutions are beyond the angle range of the actuator, which can be realized in theory but cannot be realized in actual systems. This kind of solutions is eliminated by defining the rotation angle of the steering gear. The above two kinds of solutions should be removed.

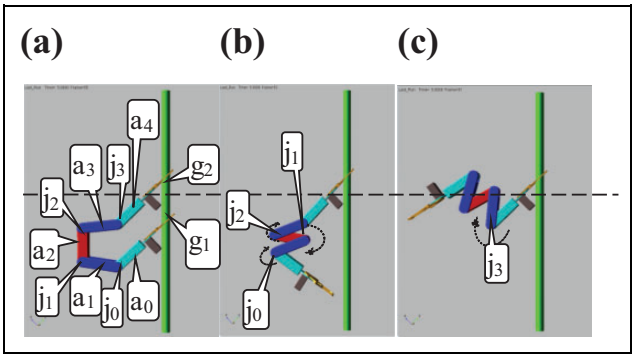

Figure 3. MPCRobot flip locomotion. (a) Loosening gripper g_1. (b) Curling up. (c) Turning over. MPCRobot: micro pole-climbing robot.

Climbing cycle for locomotion

MPCRobot climbing a pole has two gaits: the flipping-over gait and the inchworm gait. The energy consumed with the inchworm gait is the larger than the flipping-over gait.[13] MPCRobot is used for power line monitoring (with cameras and sensors) and lightning rod detection. This kind of working occasions have enough working space, so this article only discusses the flipping-over gait.

In the process of continuous climbing, the robot's posture is alternately forward and backward. In this article, the upright posture is defined as the state of g_1 below g_2, otherwise defined as an inverted posture. The self-continuous climbing process with controllable strides is decomposed into two stages: flip and stride.

Flip locomotion

The flip locomotion consists of three steps: loosening gripper g_1, curling up, and turning over, as shown in Figure 3.

Firstly, gripper g_1 is loosened, and gripper g_2 is used as the fixed end of the robot, as shown in Figure 3(a). Secondly, the robot's joints j_0, j_1, and j_2 rotate to achieve a curling posture, as shown in Figure 3(b). After the robot curls up, the overall length of the robot is greatly reduced, so as to avoid the instability of the robot caused by the excessive torque of the grasp during the overturning process. Thirdly, the robot turns over by rotating j_3 in a curled state, as shown in Figure 3(c).

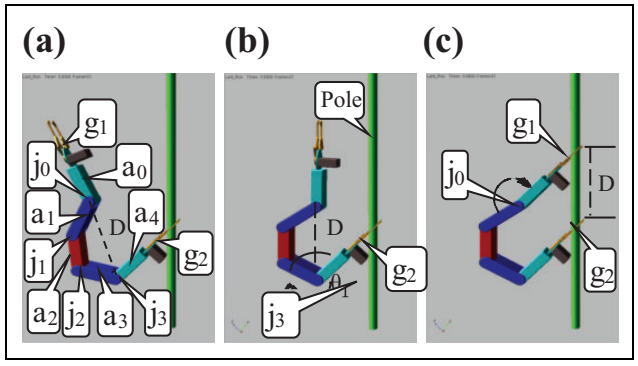

Figure 4. MPCRobot stride locomotion. MPCRobot: micro pole-climbing robot. (a) generating D. (b) paralleling. (c) grabbing with.

Stride locomotion

The robot continues to perform stride locomotion after the flip locomotion. In the process of continuous climb, the robot will be alternatively in the upright posture and inverted posture. Whether in the upright or inverted postures, the inverse kinematic solution of stride is invariable. The obtained θ_1, θ_2, and θ_3 are used to control the rotations of j_0,j_1, and j_2 (in the upright posture) or the rotations of j_3, j_2, and j_1 (in the inverted posture), respectively.

After experiencing a row of gesture in Figure 3, the robot is in the inverted posture. θ_1, θ_2, and θ_3 are used to control the rotations of j_3, j_2, and j_1. The stride locomotion consists of three steps: the determination of the stride parameter D, the adjustment of the stride posture, and the clamping of the gripper g_1, as shown in Figure 4.

First, inputing the expected stride D and using equations (5) to (11), θ_2 and θ_3 can be calculated according to angle θ_1. The robot's joints j_1 and j_2 rotate according to θ_2 and θ_3, and then a_1, a_2, and a_3 generate D, as shown in Figure 4(a).

Second, by adjusting j_3, the robot keeps the line D between j_0 and j_3 parallel to the climbing pole, as shown in Figure 4(b). When the climbing pole is perpendicular to the ground and the angle between a_3 and the ground reaches $\theta_1 + 90°$, D is exactly parallel to the climbing pole. The real-time angle between a_3 and the ground is measured by an accelerometer mounted on a_3.

Finally, the robot adjusts the attitude of the gripper g_1 by rotating j_0 and grabbing the climbing pole with g_1, as shown in Figure 4(c). For climbing robots, it is very important for the gripper to grasp the climbing pole accurately and firmly. Unreliable clamping will cause robot's falling and serious damages. Traditional calibration schemes use infrared, laser, ultrasound, and other ranging sensors or cameras.[20–22] By judging the relative position between the gripper and the pole, the robot is guided to realize alignment between gripper and climbing pole. Such schemes require more complex processing and fusion of data from sensors, which increase the cost, size, and weight of robots. This article presents an autonomous gripping scheme based on robot geometry structure, which does not require the use

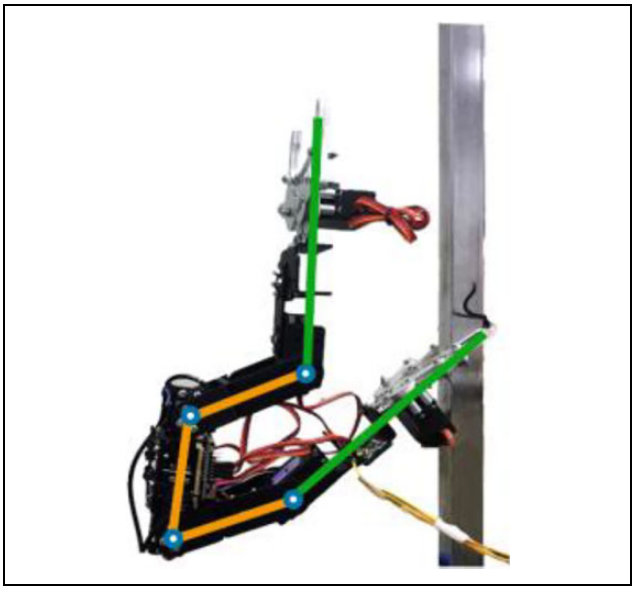

Figure 5. MPCRobot prototype. MPCRobot: micro pole-climbing robot.

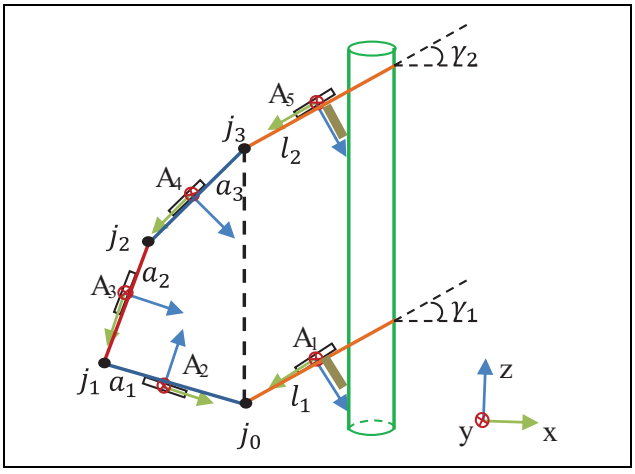

Figure 6. Installation diagram of acceleration sensors.

of additional distance measuring sensors. Two supports h_1 and h_2 are added to two grippers g_1 and g_2 to assist the grippers to grasp the pole, as shown in Figure 6(c). With the help of accelerometers mounted on g_1 and g_2, the robot can clamp the vertical climbing pole automatically when two grippers g_1 and g_2 are parallel to each other.

Prototype and experiment

Robot prototype

We designed MPCRobot prototype, as shown in Figure 5. The prototype weighs 1.07 kg (including a battery), and it is 600 mm long when fully extended. The specific size is shown in Table 2. Constrained by the robot's current structure, a single span of the robot is 8–23 cm. According to the results of the force analysis, the TBS2701 steering gear (its

Table 2. Dimensions of MPCRobot components.

Component	a_0	a_1	a_2	a_3	a_4	h_1	h_2	g_1	g_2
Length (mm)	82	84	81	84	82	40	40	110	110

MPCRobot: micro pole-climbing robot.

main parameters are listed in Table 3) was selected as the joint motor. This motor has a maximum rotation angle of 270° and can operate in joint mode, in which j_0, j_1, j_2, and j_3 can be conveniently located at any angle position. MPCRobot realizes an automatic pole climbing.

To enable the robot to sample the angle relative to the ground in real time, micro electro mechanical systems (MEMS) three-axis accelerometers (MPU6050; InvenSense Inc., Sunnyvale, USA) are equipped on l_1, a_1, a_2, a_3, and l_2, respectively, named A_1, A_2, A_3, A_4, and A_5, as shown in Figure 6. The accelerometers can measure acceleration along their own axes in the coordinate system. Accelerometer measurements provide an absolute reference for the pitch-and-roll components of the estimated orientation.[25] (x_{Ai}, y_{Ai}, z_{Ai}), $(i = 1,2,3,4,5)$ denotes the gravitational acceleration component of A_i $(i = 1, 2, 3, 4, 5)$ along its own axes x, y, and z. The full measuring range of the acceleration A_i $(i = 1, 2, 3, 4, 5)$ is ± 2 g. The measurements (x_{Ai}, y_{Ai}, z_{Ai}), $(i = 1,2,3,4,5)$ derived from A_i $(i = 1, 2, 3, 4, 5)$ are used to calculate the current attitude of the robot. (x_{A1}, y_{A1}, z_{A1}) is used to adjust (x_{A5}, y_{A5}, z_{A5}) by rotating j_3 to ensure that l_2 is parallel to l_1. $(x_{Ai}, y_{Ai}, z_{Ai})(i = 2, 3, 4)$ is used to adjust the attitude of a_{i-1} by rotating j_{i-2} (see section "Joint PID control parameters").

Joint PID control parameters

Overall system with proposed control strategy. Because the steering gear has a dead zone and a hysteresis in control, some control strategies based on proportional–integral–derivative (PID) control theory are developed to reduce the angular velocity fluctuation of a five-bar mechanism driven by the steering gear.[26] Figure 7 shows the overall system with the proposed control strategy, in which the control parameters are the proportional gain K_P, the integral gain K_I, and the derivative gain K_D. $\beta_i^{'}$ can be obtained by accumulating θ_i $(i = 1,2,3)$, which is calculated by the D-H method. $\beta_i^{'}$ can be expressed as follows

$$\beta_k^{'} = 90 + \sum_{i=1}^{k} \theta_i \; k = (1, 2, 3) \tag{13}$$

$$-3\pi + 90 \le \beta_k^{'} \le 3\pi + 90 \tag{14}$$

β_k is calculated from $(x_{Ai}, y_{Ai}, z_{Ai})(i = 2, 3, 4)$ by the accelerometers A_2, A_3, and A_4 using the angle transformation, which can be presented as

$$\beta_k = F\left(\tan^{-1}\left|\frac{x_{Ai}}{z_{Ai}}\right|\right) = \begin{Bmatrix} \tan^{-1}\left|\frac{x_{Ai}}{z_{Ai}}\right| & x_{Ai} > 0,\ z_{Ai} > 0 \\ \pi - \tan^{-1}\left|\frac{x_{Ai}}{z_{Ai}}\right| & x_{Ai} > 0,\ z_{Ai} < 0 \\ -\pi + \tan^{-1}\left|\frac{x_{Ai}}{z_{Ai}}\right| & x_{Ai} < 0,\ z_{Ai} < 0 \\ -\tan^{-1}\left|\frac{x_{Ai}}{z_{Ai}}\right| & x_{Ai} < 0,\ z_{Ai} > 0 \\ 0 & x_{Ai} = 0,\ z_{Ai} > 0 \\ \pi & x_{Ai} = 0,\ z_{Ai} < 0 \\ \pi/2 & x_{Ai} > 0,\ z_{Ai} = 0 \end{Bmatrix} \tag{15}$$

β_k is subtracted from $\beta_i^{'}$, and the resulting error $\Delta\beta$ is sent to the Ziegler–Nichols controller. The parameters of K_P, K_I, and K_D can be obtained according to the Ziegler–Nichols controller.[27,28] $\Delta\beta$ is presented as

$$\Delta\beta = \beta_k^{'} - \beta_k + 2\pi j \; \mathrm{j} \in \{-2, -1, 0, 1, 2\} \tag{16}$$

$$-\pi \le \Delta\beta \le \pi \tag{17}$$

PID controller parameters. The stabilization time of each adjustment of the steering gear is 1.2 s. The sampling time of the controller is set to 1.2 s. In order for θ_1 to produce equal amplitude oscillation, let the value of K_c be 4.3. By doing so, an approximate equal amplitude oscillation shown in Figure 8 can be obtained. The oscillation period T_c tends to be stable after T_{c3}, and $T_c = 11.5$ s can be extracted from Figure 8. According to Table 4,[29] the parameters of PID are $K_P = 2.6$, $K_I = 0.45$, and $K_D = 3.59$.

PID testing. Experimental conditions are as follows: the angle θ_1 is set to 128°, and the steady-state errors of θ_1 with and without PID are shown in Figure 9. Mean absolute deviation with and without PID are 0.262 and 0.350, respectively. It shows that the precision of PID control is higher than proportional control. Standard deviation with and without PID are 0.348 and 0.446, respectively. It can be seen that the stability of the PID algorithm is improved. The proportion of steady-state error of using PID within ($\pm 0.4°$) is increased, which is 58% higher than that without PID algorithm. The average execution time is about 17 s.

When θ_1 reaches the set angle, it produces the jitter of the robot due to the continuous fine-tune in the range of a steady-state error. Therefore, the rule is set as follows: when the measured steady-state error is less than 0.3° for two consecutive actions, the adjustment is ended.

Clamping force of the grippers

Gripper force analysis mode. The grippers need to fix the robot effectively on the pole to avoid sliding. The force analysis model of gripper is derived based on diagram, as shown in Figure 10. The gripper has four main force points

Table 3. Main parameters of TBS2701 steering engine.

Product model	Nominal voltage (V)	Max torque (kg cm)	Nominal speed (s/60°)	Rotate angle	Resolution ratio	Mass (g)	Control mode
TBS2701	5–8.4	15	0.16	0–270°	0.24°	60	PWM

PWM: pulse width modulation.

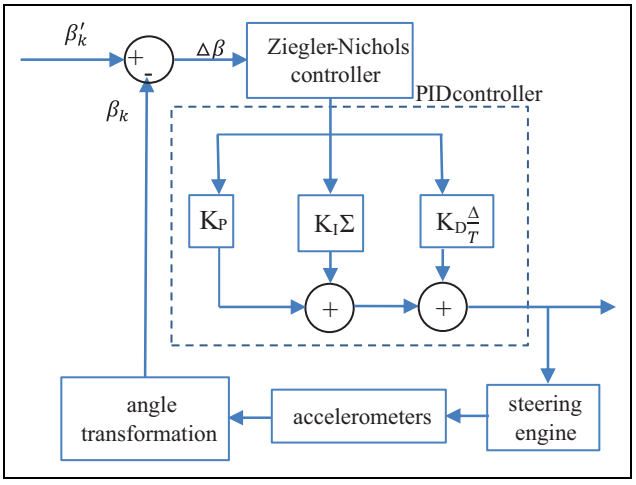

Figure 7. Overall system with the proposed control strategy.

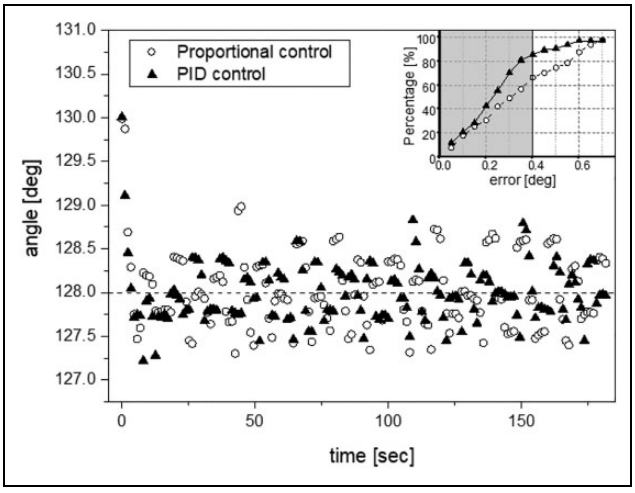

Figure 9. Comparison of steady-state error with and without PID algorithm. PID: proportional–integral–derivative.

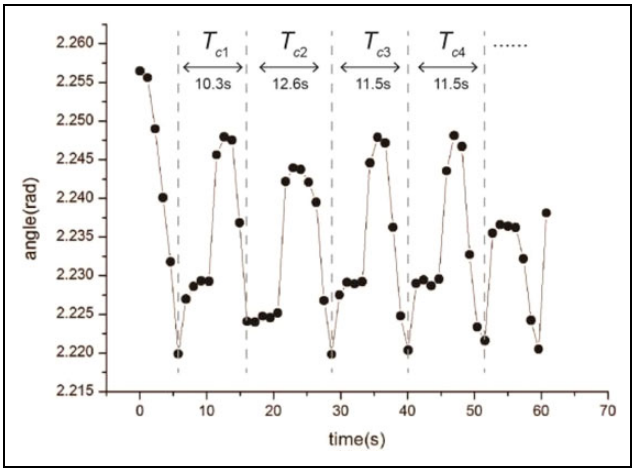

Figure 8. Approximate equal amplitude oscillation under $K_c = 4.3$.

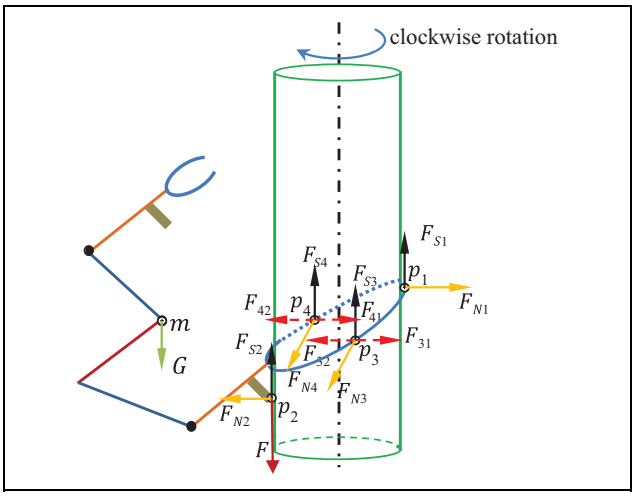

Figure 10. Gripper force analysis.

Table 4. Main parameters of the steering engine.

Controller	Calculating characteristic parameters				
	K_P	T_n	T_v	K_I	K_D
P	0.5 K_c	—	—	—	—
PD	0.8 K_c	—	0.12 T_c	—	$K_P \bullet T_v$
PI	0.45 K_c	0.85 T_c	—	$\frac{K_p}{T_n}$	—
PID	0.6 K_c	0.5 T_c	0.12 T_c	$\frac{K_p}{T_n}$	$K_P \bullet T_v$

PID: proportional–integral–derivative.

of p_1, p_2, p_3, and p_4. p_1 and p_2 are subjected to upward friction forces of F_{S1} and F_{S2} and outward support forces of F_{N1} and F_{N2} perpendicular to the rod, respectively. p_3 and p_4 are subjected to upward friction forces of F_{S3} and F_{S4} and outward support forces of F_{N3} and F_{N4} perpendicular to the rod, respectively. F_{31} and F_{42} are the friction forces when the gripper rotates clockwise with respect to the pole. F_{32} and F_{41} are generated when the gripper rotates counterclockwise. F_{31} and F_{42} prevent the gripper from turning clockwise. F_{32} and F_{41} prevent the gripper from turning counterclockwise.

Table 5. Results of anti-slip load capacity test.

Material	Diameter (mm)	Critical value of F (N)
PVC	24	21.1
Iron	24	49.2
PVC (with rubber pad)	24	52.3
Wood	24	96.6

In order to stay on pole, equation (18) can be obtained

$$G < F_{S1} + F_{S2} + F_{S3} + F_{S4} \tag{18}$$

$$F_{S1} = \mu_S F_{N1} \tag{19}$$

$$F_{S2} = \mu_S F_{N2} \tag{20}$$

$$F_{S3} = \mu_S F_{N3} \tag{21}$$

$$F_{S4} = \mu_S F_{N4} \tag{22}$$

where G is the gravity of the robot at the center of mass m and μ_S is the static coefficient of friction between gripper and pole. The friction forces of F_{S1}, F_{S2}, F_{S3}, and F_{S4} increase with the increases of F_{N1}, F_{N2}, F_{N3}, and F_{N4} which are related to the clamping force of the gripper. Above is the static analysis of the gripper force, while the dynamic analysis process is more complex.

Physical testing. In physical testing, the clamping forces of the gripper to hold the pole with different materials (wood, iron, polyvinyl chloride (PVC), and PVC with rubber pad) are tested. The gripper is made of aluminum alloy material. The maximum tension angle of gripper is 55 cm. The maximum torque of the motor driving the gripper is 15 kg cm. The experimental process is as follows: the lower gripper of the robot is clamped, the upper gripper is suspended, and the vertical downward pulling force F is applied at p_2. F was measured with a tensiometer (Edinburgh Instrument, HP-500, indexing value 0.1 N). Increasing F until the lower gripper slips from the climbing rod, and record the value of the pulling force (called critical value of F) at this time. The experimental data are shown in Table 5.

In the test, the clamping experiments of pole climbing with the same diameter, but different materials were carried out. The critical force of the gripper on PVC material is 21.1 N. In order to increase the critical force on the PVC pole, a layer of rubber was wrapped around the PVC pole. From Table 5, the addition of rubber layer did increase the critical value from 21.2 N to 52.3 N, which is due to the increase of sliding friction coefficient between the materials. The experimental results show that increasing the friction coefficient between the gripper and the rod can improve F, which means an increased load capacity of the overturning robot.

Pole-climbing experiment

This article designs an experiment to test the climbing speed and the accuracy of step distance, respectively. On a vertical climbing pole, the robot makes repeated strides with a stride of 8–23 cm. The self-continuous climbing process with controllable stride is shown in Figure 11. The flip locomotion, that is, loosening gripper g_1, curling up, and turning over, is shown in Figure 11(a), (b) and (c), respectively. The stride locomotion, that is, the determination of the stride parameter D, the adjustment of the stride posture, and the clamping of the gripper g_1, is shown in Figure 11(e), (f) and (g), respectively.

The time consumed and the errors of stride are recorded, respectively.

Stride experiment. The measurement started with a curl-up (Figure 11(c)) and ended with grabbing the climbing pole with g_1 (Figure 11(f)). In the physical testing, a single stride was 8–23 mm, and the step length was 1 mm. Sixteen groups of experiments were conducted, and each group was repeated 10 times. Statistics of time consumed for single stride are given in Figure 12. "Percentage" in Figure 12 represents the percentage of the total number of experiments that took time in the abscissa range, and "cumulative percentage" represents the percentage of all results that were less than or equal to the total number of experiments that took time in the abscissa range.

In the test, the step length of each group of experiments was different (from 8 mm to 23 mm), which resulted in different execution time for the robot to complete the step action. The proportion of complete action within 40 s was close to 90%, and the average time consumed was about 27 s.

Flip experiment. When each stride is completed, the distance between two grippers is measured with a ruler. Compared with the set distance, the relative error statistics of the single stride can be obtained, as shown in Figure 13. "Percentage" in Figure 1 indicates the percentage of errors in the abscissa range to the total number of experiments, and "cumulative percentage" represents the percentage of all results less than or equal to the total number of current abscissa errors.

The range of a single stride is 8–23 cm. The maximum relative error is 4.6%, and the average error is 2.8%. The single span of MPCRobot is 8–23 cm. The absolute error of a single span is 0.22–0.64 cm.

Comparison of climbing robot

A comparison of climbing robot is shown in Table 6. Pole size indicates the cross section of the climbing pole. The pole size that MPCRobot can clamp is the smallest so as to tighten the pole with smaller diameter. The maximum load of Treebot is 2.9 times its own weight, while the maximum load of MPCRobot is 3.5 times its own weight. This is due

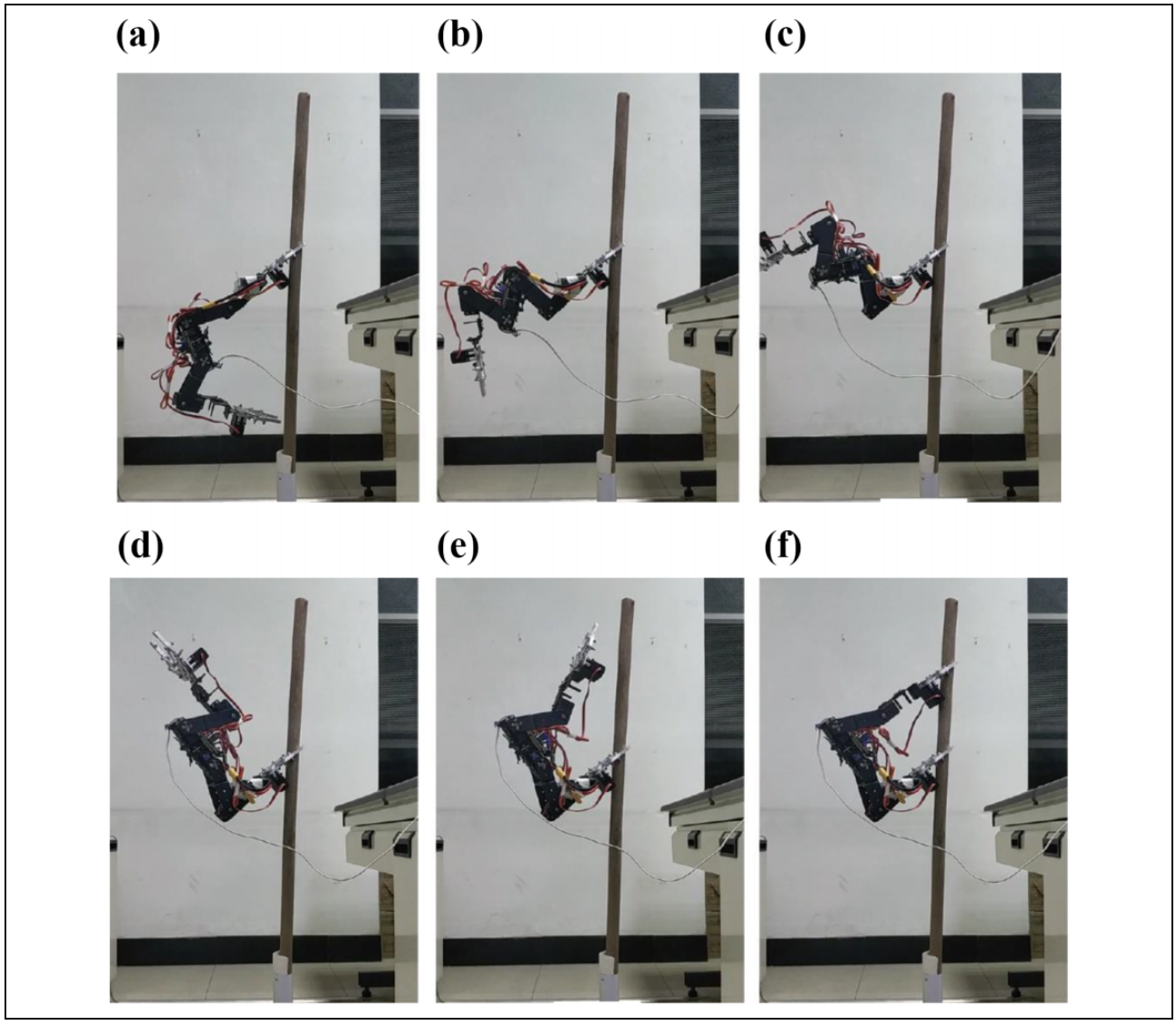

Figure 11. Continuous climbing steps of MPCRobot. MPCRobot: micro pole-climbing robot. (a) Loosening gripper. (b) Curling up. (c) Turning over. (d) generating D. (e) paralleling. (f) grabbing with.

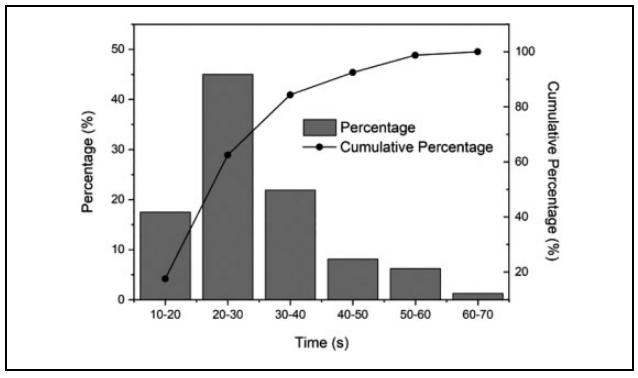

Figure 12. Single stride time chart.

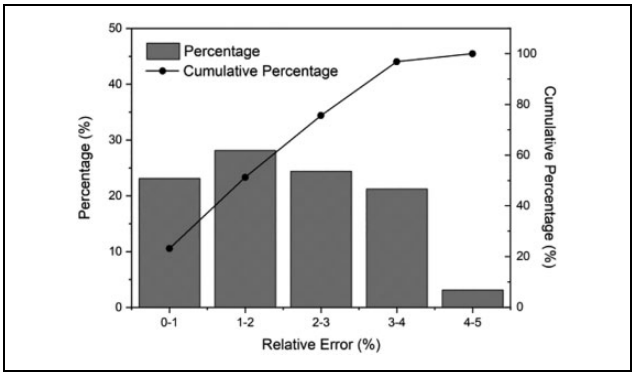

Figure 13. Statistics of relative error of single stride.

to the triangular structure consisting of a gripper, a support structure, and a climbing pole (see Figure 1), which can provide stable support for the robot. The single span of MPCRobot is 8–23 cm, and relative error of stride is 2.8%. Then the absolute error of a single span is 0.22–0.64 cm. MPCRobot striding has high accuracy in each step

Table 6. Comparison of main parameters of robot.

	Mass (kg)	Full expansion length (cm)	Max load (kg)	Max speed (cm/min)	Relative error of stride (%)	Pole size (mm)
Pipelinebot[30]	0.46	22	—	67.2	—	Φ50–60
Treebot[21]	0.6	66.5	1.75	22.4	—	Φ64–452
Minibot[31]	0.75	49	—	—	—	Φ40
MPCRobot	1.07	60	3.79	48	2.8	Φ8–55
Shady3D[10]	1.34	25	—	20.4	—	19 × 19 (Rectangular cross section)
Climbot[13]	17.5	152	—	220	—	Φ50–120
3DClimber[17]	42	60	—	100	—	Φ200–350

length. Thus, MPCRobot can be used to climb small diameter poles to complete fixed-point monitoring tasks, such as power line monitoring (with cameras and sensors), truss climbing and lightning rod detection, and other working occasions.

Conclusions

A 3-D model of MPCRobot was presented. It consists of five-bar linkages, four joints, two supports, and two grippers. A supporting structure was installed at the joint of each gripper to assist the robot to clamp the climbing pole. The support structure improves the load capacity of the robot. The maximum load of MPcrobot is 3.5 times its own weight. To enable the robot to sample the angle relative to the ground in real time, MEMS three-axis accelerometers are equipped on MPCRobot. Accelerometer measurements provide an absolute reference for the pitch and roll components of the estimated orientation, which are used as feedback input signal of PID algorithm.

A strategy of climbing pole is proposed, which has high precision in each stride. The climbing pole strategy includes the following sections: a D-H model is established and the inverse kinematic solution is analyzed; the flip locomotion is analyzed; and the parameters of K_P, K_I, and K_D in the PID control method are obtained according to the Ziegler–Nichols controller.

The MPCRobot prototype was thus developed and tested for pole climbing. By using this strategy of climbing pole, the self-continuous climbing with controllable stride is realized, and the angular velocity fluctuation of the five-bar mechanism driven by steering gear is reduced. The average time of a single step is 27 s, the maximum relative error of step distance is 4.6%, and the average relative error is 2.8%. These results confirm that the structure scheme and the strategy of climbing pole are feasible.

Declaration of conflicting interests

The author(s) declared no potential conflicts of interest with respect to the research, authorship, and/or publication of this article.

Funding

The author(s) received no financial support for the research, authorship, and/or publication of this article.

ORCID iD

Du Qiaoling https://orcid.org/0000-0002-4521-8041

References

1. Goldman G and Hong D. Considerations for finding the optimal design parameters for a novel pole climbing robot. In: *32nd Annual mechanisms and robotics conference*, New York, USA, 03–06 August 2008.
2. Haynes GC, Khripin A, and Lynch G. Rapid pole climbing with a quadrupedal robot. In: *IEEE International conference on robotics and automation*, Kobe, Japan, 12–17 May 2009.
3. Song W, Li Y, Wan L, et al. Research of underactuated gripper for power tower climbing robot. *Chinese J Sci Instru* 2015; 36(Supplement): 6.
4. Zahra BK, Hasib UM, Razu A, et al. Electrical Pole climbing robot for wiring and repairing distribution lines. In: *18th International conference on computer and information technology*, Dhaka, Bangladesh, 21–23 December 2015.
5. Allan JF, Lavoie S, and Reiher S. Climbing and pole line hardware installation robot for construction of distribution lines. In: *1st International conference on applied robotics for the power industry*, Montreal, CANADA, 05–07 October 2010.
6. Faizal MIN, Othman WAFW, and Hassan SSNA. Development of pole-like tree climbing robot. In:*5th IEEE international conference on control system, computing and engineering (ICCSCE)*, Batu Ferringhi, Malaysia, 27–29 November 2015.
7. Li Z, Ge Z, Cheng F, et al. Design and Implementation of a new type of climbing robot for Living trees. *Wood Proc Mach* 2016; 27(01): 32–34+56.
8. Fauroux J and Morillon J. Design of a climbing robot for cylindro-conicpoles based on rolling self-locking. *Ind Robot* 2010; 37(3): 287–292.
9. Zhu H, Guan Y, and Su M. Evaluation of graspable region and selection of footholds for biped pole-climbing robots. In: *2014 IEEE international conference on robotics and biomimetics (ROBIO)*, Bali, Indonesia, 05–10 December 2014.

10. Yoon Y and Rus D. Shady3D: a robot that climbs 3D trusses. In: *IEEE international conference on robotics and automation*, Rome, Italy, 10–14 April 2007.
11. Zhang L, Ge Z, Liu C, et al. Review on key technologies of rod climbing robot. *Comput Meas Control* 2018; 26(01): 1–5.
12. Chen G, Cao H, Yang H, et al. Research status and outlook of rod climbing robots. *Ordnanc Indus Autom* 2018; 37(03): 21–31.
13. Guan Y, Jiang L, Zhu H, et al. Climbot: a bio-inspired modular biped climbing robot—system development, climbing gaits, and experiments. *J Mech Robot* 2016; 8(2).
14. Chen W, Gu S, and Zhu L. Representation of truss-style structures for autonomous climbing of biped pole-climbing robots. *Robot Auton Syst* 2018; 101: 126–137.
15. Chen S, Zhu H, and Guan Y. Collision-free single-step motion planning of biped pole-climbing robots in spatial trusses. In: *IEEE International conference on robotics and biomimetics (ROBIO)*, Shenzhen, China, 12–14 December 2013.
16. Zhou X, Jiang L, and Guan Y. Energy-optimal motion planning of a biped pole-climbing robot with kinodynamic constraints. *Industr Robot Int J Robot Res Appl* 2018; 45(3): 343–353.
17. Tavakoli M, Marques L, and Almeida ATD. 3DCLIMBER: climbing and manipulation over 3D structures. *Mechatronics* 2011; 21(1): 48–62.
18. Sadeghi A, Moradi H, and Ahmadabadi MN. Analysis, simulation, and implementation of a human-inspired pole climbing robot. *Robotica* 2012; 30: 279–287.
19. Tavakoli M, Zakerzadeh MR, and Vossoughi GR. A hybrid pole climbing and manipulating robot with minimum DOFs for construction and service applications. *Ind Robot* 2005; 32(2): 171–178.
20. Tavakoli M, Marques L, De Almeida AT, et al. Self calibration of step-by-step based climbing robots. In: *IEEE/RSJ International Conference on Intelligent Robots and Systems*, St Louis, MO, USA, 10–15 October, 2009, pp. 3297–3303.
21. Lam TL and Xu Y. Treebot: autonomous tree climbing by tactile sensing. *Int Conf Robot Autom* 2011; 789–794.
22. Tavakoli M, Marques L, De Almeida AT, et al. A low-cost approach for self-calibration of climbing robots. *Robotica* 2011; 29(01): 23–34.
23. Guo Z, Cui T, Lv X, et al. Inverse kinematics of 6-DOF manipulator. *Agricult Mech Res* 2016; 38(12): 51–55.
24. Guo W, Li R, and Cao C. Innovative closed-form solution and workspace analysis for a 5-DOF manipulator. *J Huazhong U Sci (Natural Science Edition)* 2015; 43(S1): 14–18.
25. Chen Y, Xu L, Zhao L, et al. Motion recognition based on a three-axis accelerometer. In: *Proceedings of the 32nd Chinese control conference*, Xi'an, China. 26–28 July 2013.
26. Wan Y, Li C, Guo H, et al. A steering gear system controller in missiles based on the fractal modified PID algorithm. *J Xidian Univ* 2007; 34(1): 145–148.
27. Reis MRC, Silva FS, Araujo WRH, et al. Speed control for direct current moto r using optimization tuning for PID controller. In: *2016 - International conference on environment and electrical engineering*, Florence, Italy, 7–10 June 2016.
28. Oveisi A and Gudarzi M. Adaptive sliding mode vibration control of a nonlinear smart beam: a comparison with self-tuning Ziegler-Nichols PID controller. *J Low Freq Noise V A* 2013; 32(1): 41–62.
29. Dong F. PID controller parameter tuning based on Ziegler-Nichols rule. *Autom Instrument* 2015; (07): 105–106.
30. Luo J. *Analysis of dynamic characteristics and structural design of pipeline climbing robot*. Wuhan: Wuhan University of Science and Technology, 2015.
31. Cai C, Zhu H, Jiang L, et al. A biologically inspired miniature biped climbing robot. In: *International conference on mechatronics and automation*, Changchun, China, 9–12 August 2009, pp. 2653–2658. IEEE.